Nagoya Multi-Directional Muon Telescope

Cosmic-Ray Research Section,
Solar-Terrestrial Environment Laboratory,
Nagoya University, Nagoya, 464-8601 Japan

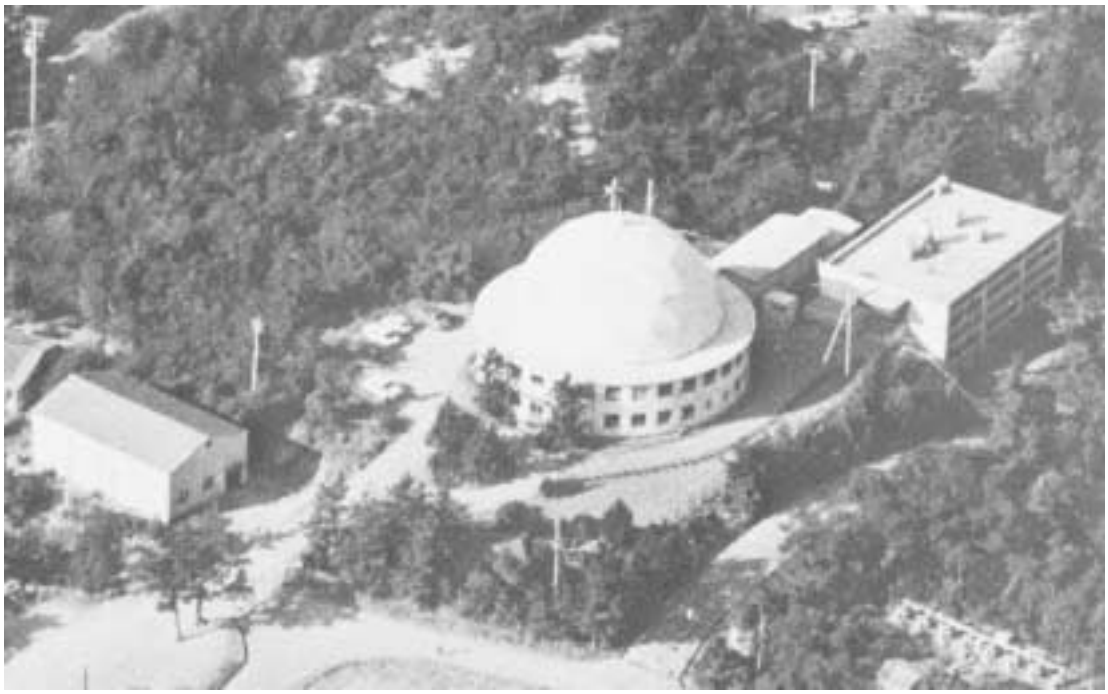

CONTENTS

I. INTRODUCTION

Multi-Directional Cosmic-Ray Muon Telescope at Nagoya was planned and constructed as a part of Japanese program for the International Active Sun Year (IASY). The construction of the telescope as well as the building for it, was started in the summer of 1968. The building was completed in March 1969, and the telescope was completed in autumn of 1969. After careful check of the whole system, continuous observation of the cosmic-ray intensities was started in October 1970 and has been continued thereafter. This telescope has an effective area of 36 m^2 in which 9 m^2 has the role as the muon monitor in Japan.

The geographical and geomagnetic coordinates of the observation site are summarized in Table I. Average variations of the climate at Nagoya, such as the temperature and the atmospheric pressure, are shown in Fig. 1. The building which houses the telescope was built near the top of a hill in the University campus beside the dome for a Cerenkov telescope built in 1959 as shown in Fig. 2. The building has an area of 152 m^2 with a thin slate roof and heat insulation structure as shown in Fig. 3. The telescope was constructed inside a thermostatic chamber (7.2×7.2×4.3 m^3) built in an air conditioned room (117 m^2).

Table I. Locality of observation site

Geographical Latitude; 35°09'N, Longitude; 136°58'E Altitude; 77 m above sea level
Geomagnetic Latitude; 24.7°N Declination; 6.44°W, Inclination; 48.25°N

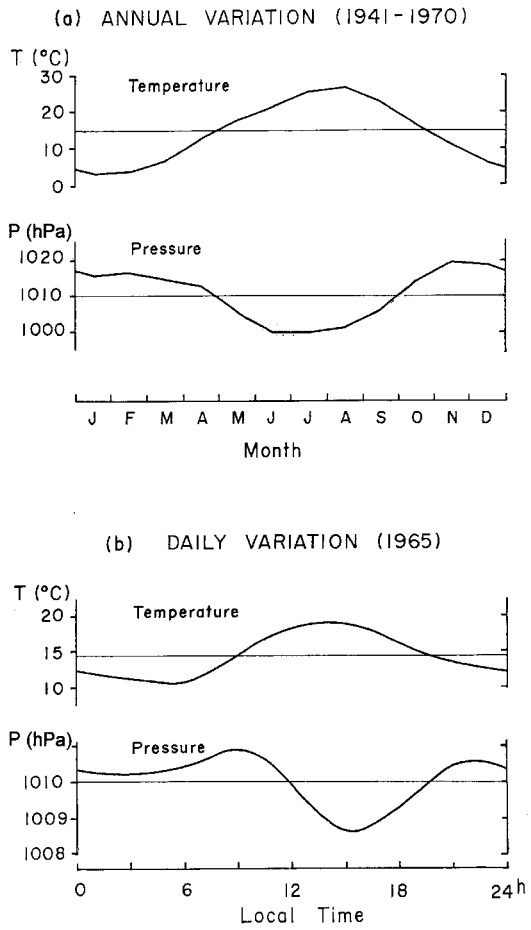

Fig. 1. a) Average annual variations of the temperature and the atmospheric pressure at Nagoya for 1941-1970

b) Average daily variations of the temperature and the atmospheric pressure at Nagoya for 1965

Fig. 2. Aerial view of STEL: The building for the multi-directional telescope is at the left side of the photograph, with dome for the Cerenkov telescope at the center, and the laboratory office at right.

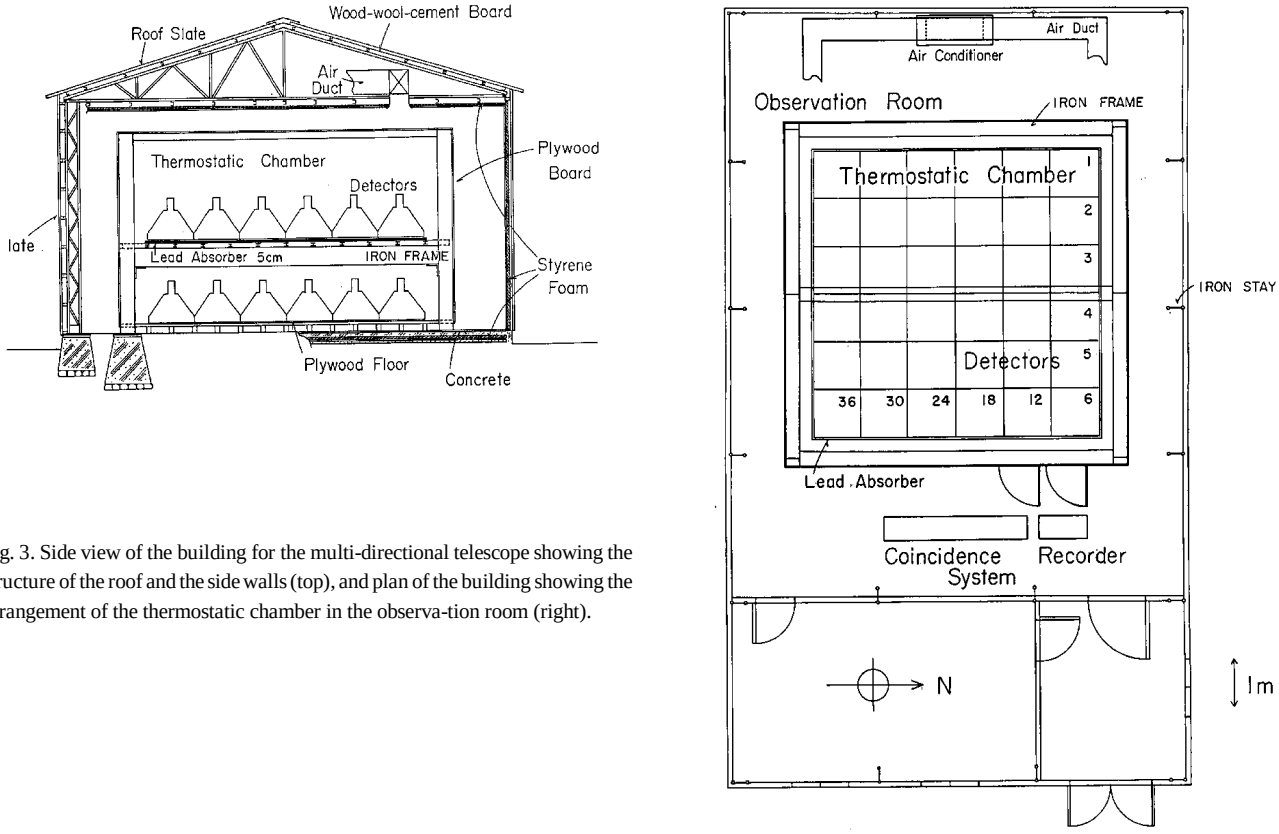

Fig. 3. Side view of the building for the multi-directional telescope showing the structure of the roof and the side walls (top), and plan of the building showing the arrangement of the thermostatic chamber in the observa-tion room (right).

II. MULTI-DIRECTIONAL MUON TELESCOPE AT NAGOYA

a. Setting of the telescope

The multi-directional muon telescope consists of 2 layers of 36 detectors as shown in Fig. 4. Two layers are separated by 1.73 m in height by means of iron frames and Pb blocks of 5 cm thickness, which are placed just underneath the detectors of the upper layer in order to absorb soft component of cosmic rays. The detector consists of a 5 cm thick plastic scintillator of 1 m^2 area, which is set at the bottom of 1.6 mm thick iron plate box and viewed by a 5" phototube *(Hamamatsu Photonics R877*). These detectors are placed in a square (6 $\times$ 6 m^2) on each layer, one side of which is set along the geographical north-south direction. Each detector is called by the number, attached in the figure, with initial *U* or *L* for the upper or lower layer *(i.e. U1, U2, ..., U36, L1, L2, ..., L3*6). Sometimes, the detectors with the initial *U* or *L* are called the upper or lower detectors. Multi-directional muon telescope is constructed by a group of sets of 2-fold coincidence between the upper and lower detectors. The selection rule of the sets is given in II-c.

b. Electronic circuits

The block diagram of the electronic circuits for the telescopeis shown in Fig. 5. Pulses from each phototube are amplified (~300) by a circuit, which is set in the phototube box. Differential pulse height distribution from a detector after amplification is shown in Fig. 6. The distribution of signal (cosmic-ray) pulses has a maximum at a certain pulse height (which is referred to as the peak pulse height) and can be discriminated from that of the noises (γ-rays etc.) by choosing a proper discrimination bias. However, the discrimination bias voltage is fixed to a preset value (~0.5V) in the present circuit, so the high tension voltage of each phototube is adjusted in turn. To compensate the differences in the sensitivities of phototubes as well as the scintillation efficiencies of detectors, the following procedure is taken for the adjustment.

i) The high tension voltage of each phototube is adjusted by inserting a proper resistor between the output of a common High Voltage (H.V.) supply and the resister network of the phototube as shown in Fig.7, so that the peak pulse height for all the phototubes coincide among them-

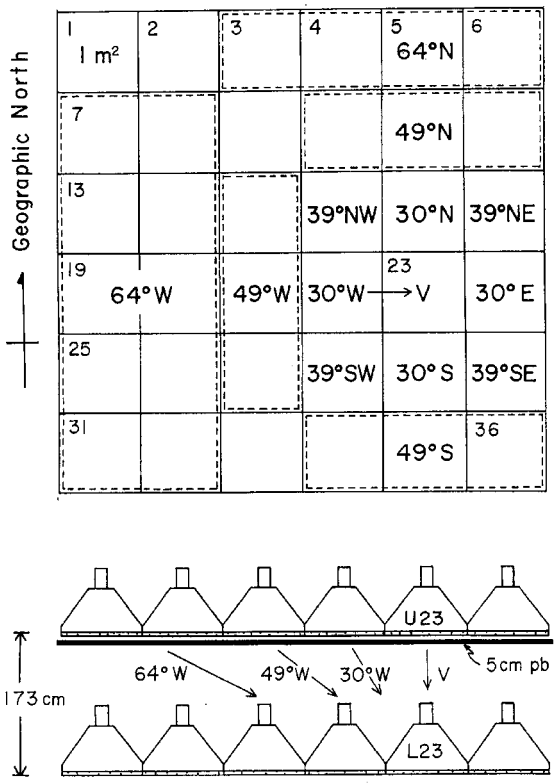

Fig. 4. Setting of the detectors in the multi-directional telescope: Numbers attached to the square denote the detector nos., and *V, 30°N etc.*, specify the name of component, relating to the upper detector in coinci-dence with *L23* detector

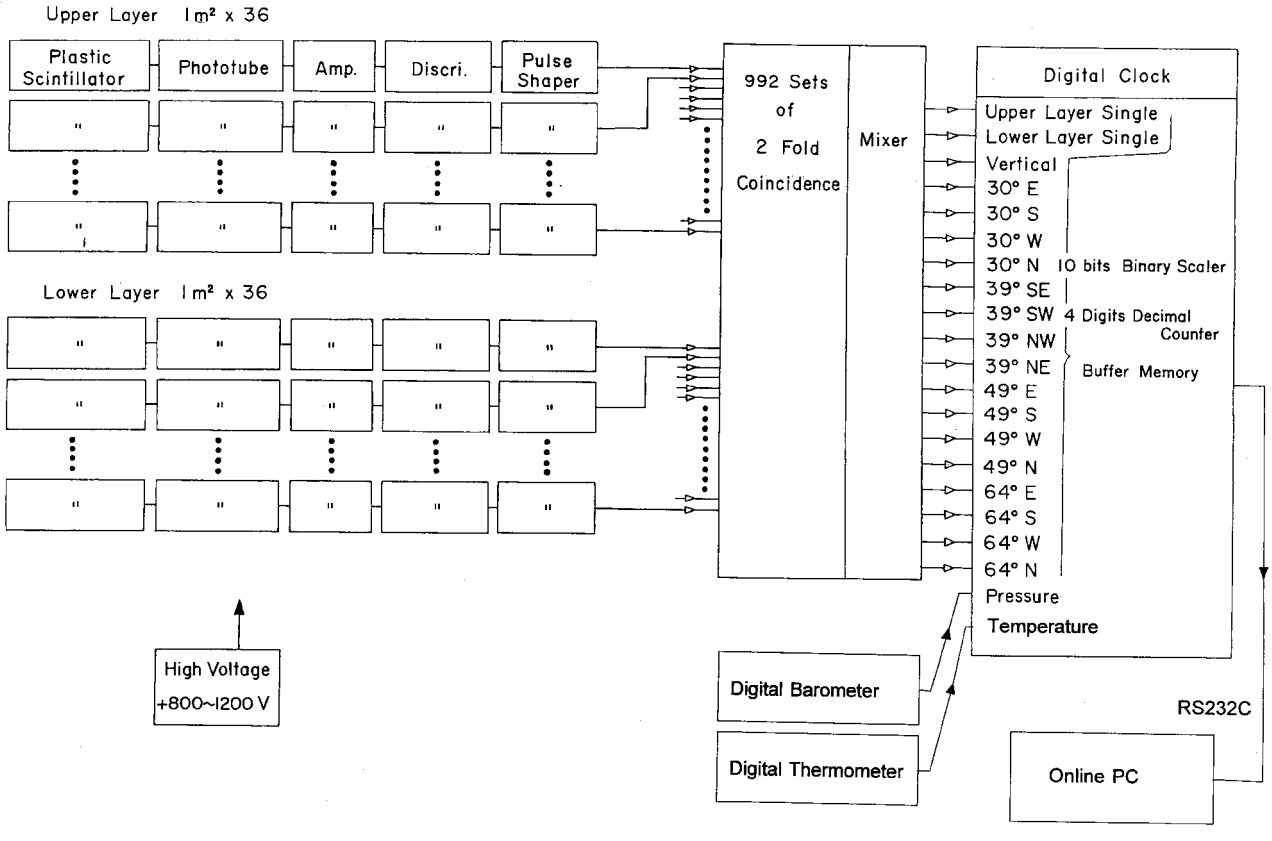

Fig. 5. Block diagram of the electronic circuits of the telescope, showing the path of signals from the detectors to the outputs of the recorder system.

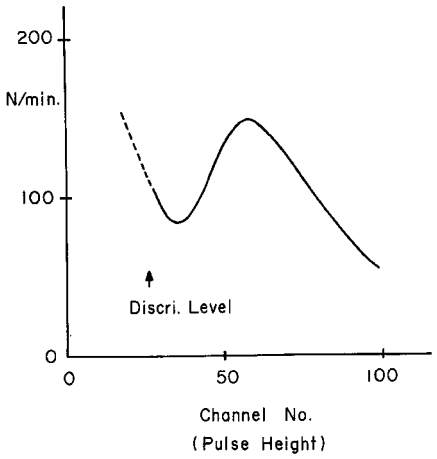

Fig. 6. Differential pulse height distribution of output pluses from this amplifier: Peak at right side is due to the cosmic-ray particles, while the rise in lower pulse height region is mainly due to background gamma-rays

selves.

ii) The counting rate for various components *(cf.* II-c) was obtained as a function of the common H.V. supply voltage, as shown in Fig. 8.

iii) In order to get the best stability for continuous observation, the voltage of the common H.V. supply should be set at a point where the slope of the curve in Fig. 8 has the minimum value. However, as seen in the figure, such a value is different for different component, and the median value for the vertical component and the single counts *(i.e.* Upper and Lower in Fig. 8) was taken as the value of the H.V. supply voltage, as shown by a straight line in the figure.

Single counting rate of one detector corresponding to this setting was about $1.1 \cdot 10^4$ c/min. in the upper layer and $0.9 \cdot 10^4$ c/min. in the lower, and the equivalent discrimination bias is shown by an arrow in Fig. 6. Temperature dependences of the scintillation efficiency, the phototube sensitivity, the gain of the amplifier and the discriminator bias

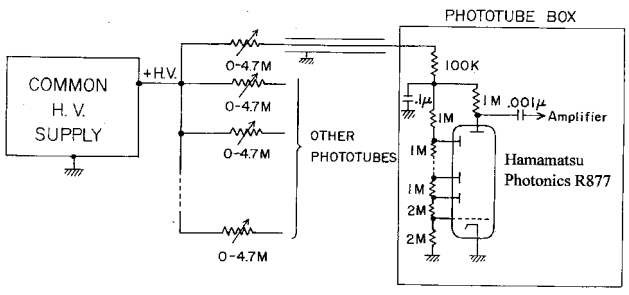

Fig. 7. Circuit to adjust the high tension voltage of phototube by vary-ing the value of resister between the common H.V. supply and the resister network of the phototube

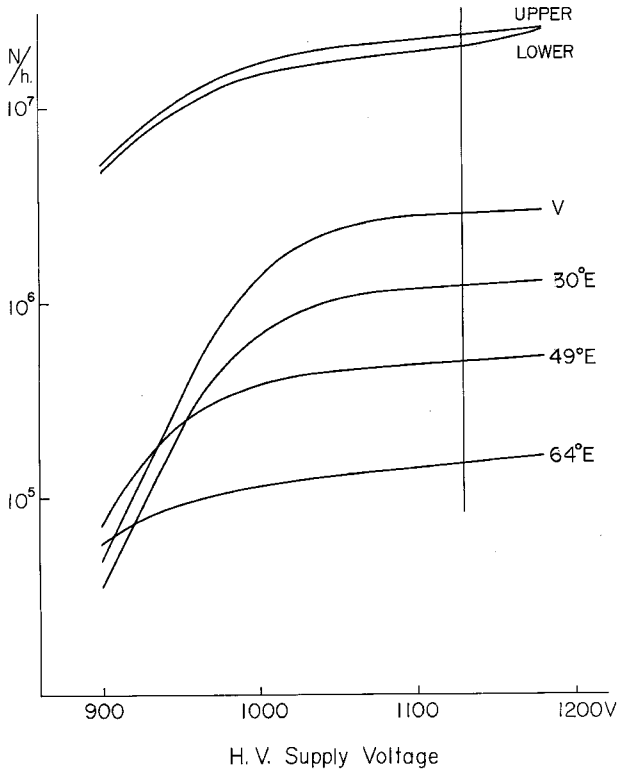

Fig. 8. Dependence of the counting rates of various components on the change of H.V. supply voltage.

were studied. It was found that these dependences produce a net change of −0.035% in the observed intensity for +1°C change in temperature.

c. Coincidence system and component telescopes

Pulses from 72 detectors in the upper and lower layers are properly fed into 992 sets of 2-fold coincidence circuits to construct 17 component of the telescope. Each component of the telescope consists of all the possible sets of 2-fold coincidence between any pair of upper and lower detectors placed in relative positions, as specified below. Taking *L23* as the position of the lower detector in Fig. 4, the relative position of the upper detector for the specified component such as *Vertical, 30°W, 39°NW, 49°W or 64°W* is defined by a square or dashed rectangle with the specified mark in the figure. Relative position for other directions is easily found from the figure. For large zenith angles, such as 49° and 64°, the dashed rectangular area larger than 1 m^2 is adopted in order to increase counting rate. It is noted, however, that this area is varied from 3 to 2 m^2 for 49° and between 10 and 3 m^2 for 64° depending on the location of the lower detector, an example of which as shown by the rectangle for *64°N* in Fig. 4.

Directional sensitivity of each component of the tele-

scope,after summing up all the possible sets of coincidence, is shown in Figs. 9 and 10. The average counting rate, the effective geomagnetic cut-off rigidity at the maximum sensitivity and the total solid angle multiplied by area ($S\Omega$) are shown in Table II, together with the number of sets of coincidence for each component. The effective cut-off rigidities were determined in considering the effect of shadow cone of cosmic-ray orbits in the geomagnetic field, which is approximated by 6 order coefficients of spherical functions *(Finch and Leaton, 1957*).

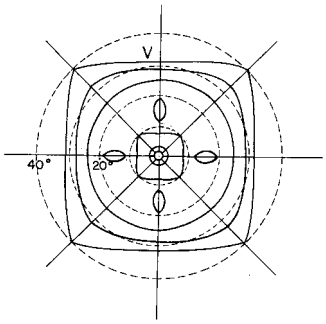

Fig. 9. Directional sensitivity of *Vertical* component is shown by con-tour lines of equal sensitivity in a polar diagram of zenith and azimuthal angles

In the table, $S\Omega$ multiplied by the square of cosine of the zenith angle (z) is also shown for a crude estimate of the cosmic-ray flux for each component. It is noted that at large zenith angles, the observed rates become larger than the expected values, which is an indication of the contamination

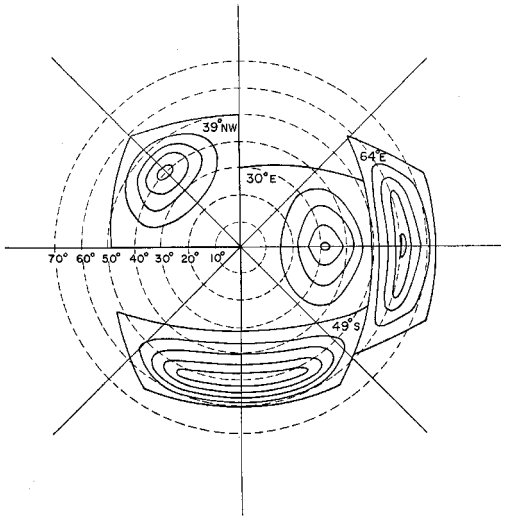

Fig. 10. Directional sensitivities of *30°E, 39°NW, 49°S* and *64°E* components are shown by contour lines of equal sensitivity in a polar diagram of zenith and azimuthal angles.xii

Table II. Geometical parametes and counting rates. Value of *N0* is that fixed for periods after Jan. 30, 1971 *(cf.*II- c).

Component	Total solidangle ×area ($S\Omega$) (m^2 *sterad*)	$S\Omega \times \cos^2 z$	Average counts *N0* (*10^6/hour)	Effective geomagnetic cut-off (GV.)	No. of 2-fold coin. sets
Vertical	9.93	9.09	2.76	11.5	36
30° North	5.23	3.97	1.25	12.9	30
30° East	5.23	3.97	1.20	16.2	30
30° South	5.23	3.97	1.23	11.3	30
30° West	5.23	3.97	1.26	9.4	30
39° NE	2.94	1.87	0.58	17.9	25
39° SE	2.94	1.87	0.58	15.0	25
39° SW	2.94	1.87	0.60	9.2	25
39° NW	2.94	1.87	0.62	11.0	25
49° North	3.37	1.58	0.49	12.9	64
49° East	3.37	1.58	0.46	21.0	64
49° South	3.37	1.58	0.48	10.9	64
49° West	3.37	1.58	0.49	9.3	64
64° North	1.50	0.33	0.14	11.0	120
64° East	1.50	0.33	0.14	25.1	120
64° South	1.50	0.33	0.14	10.8	120
64° West	1.50	0.33	0.15	8.7	120
Total	62.09	40.09	12.55	12.55	992

by shower events in the observed counts. This is due to the insufficient stopping power of 5 cm thick Pb blocks against shower particles.

d. Recording system

The output pulses from the coincidence system are fed into a recorder system *(cf.* Fig. 5). Each channel of the recorder consists of 10 bits binary scaler and 4 digits decimal counter with 4 digits buffer memory. The scaling factor *(*K) of the binary scaler is so adjusted that the counting rate of the decimal counter becomes about 8000/10 min. The accumulated counts in the decimal counter are transferred to the buffer memory once every 10 minutes and then the counter is cleared up for the next accumulation period. The contents of the buffer memories as well as the universal time *(U.T.*) code from an electronic clock are transferred by an automatic scanning circuit to an PC via a serial output of RS232C. Nineteen channels of the recorder are used to record the counting rates of the cosmic-ray intensities from 17 directions together with the total single counts of the upper and lower layers. Another channel of the recorder is used to accumulate pulse counts from a digital barometer by means of a quartz crystal resonator. The room temperature as well as the outdoor temperature are also measured by a digital electric thermometer to record with the same recording system.

e. Power supplies

In order to avoid interruption of the observation due to the electric failure, an *AC-DC-AC* converter system with a deck of floating batteries (9.2 KV AH) is used for the *AC* power supply. This system can supply 500 VA power to the telescope for 6 hours without *AC* power input. High voltage supply to the phototube is highly stabilized ($4 \cdot 10^{-4}$ % for 1V *AC* change), but has a temperature dependence of −50 mV/°C. *DC* power supplies for the amplifier and the discriminator are also stabilized for the *AC* voltage change, but have temperature dependencies of −10 and −2 mV/°C respectively. The effect of changes in the supply voltages on the counting rates was studied and it was found that the change of the power supply voltage caused by +1°C changeof the room temperature produces −0.006% change in the observed intensity.

As the logic circuits for the coincidence system as well as the recorder system are not sensitive to the change of the supply voltage, conventional stabilizers are used in the power supplies for these systems.

f. Overall stability of the telescope

High counting rate of the telescope as shown in Table II, naturally reduces the statistical fluctuations due to the finite counting rates. Then the change of counting rate due to other reasons such as the change of the pulse height distribution has much important effect on the stability of the observed rate. Instrumental fluctuations in short time interval (less than a day), is mainly originated from the change of the room temperature. In order to reduce this cause, the room temperature of the observation room is air-conditioned to 20±1°C and the temperature variation in the thermostatic chamber containing the telescope is maintained within ±0.1°C throughout the year. By this regulation of the temperature change, the observed intensity has an overall stability of ±0.01% for duration of a few days *(cf.* II-*b,* e).

The stability in longer time interval is mainly controlled by the variation in the pulse height distribution due to the fatigue of the phototube as well as the change of the scintillation efficiency. As no compensation for these effects were made, decrease less than 1% per year in the counting rate was observed.

III. REDUCTION OF DATA

a. Adoption criteria for raw data to produce hourly counts (N)

PC checks counts transferred for every 10 minutes interval whether they are inside certain limits. These limits are chosen to reject any variation of counting rates outsides of +5% and −15% of the average counting rate. Then all counts satisfying the criteria are summed up for hourly values if at least three 10 min. values pass this test, and normalized to hourly counting rates *(*n). Further, the counts are multiplied by the scaling factor *(*K) of the binary scaler to obtain the total counts *(*$N = n \times$K) for the particular hour.

b. Conversion into relative intensity (W) by means of Natural Logarithmic Representation

Accumulated counts per hour *(*N) are then converted into the relative intensity *(*W) using the Natural Logarithmic Representation *(Wada, 1957*) as follows:

$$W = 10^2 \times \ln (N/N0) + WL \quad \text{in units of \%} \qquad (1)$$

where *N0* is the average counting rate and *WL* (15.0%) is artificially added to make the values of Walways positive.

c. Pressure correction and the barometer corrected relative intensity (W_P)

The counting rate (N_P) of the digital barometer is converted into atmospheric pressure (*P*) by using a conversion formula and a set of calibration coefficients (*A*, *B*, and *C*) as,

$$P = A + B \cdot N_P + C \cdot N_P^2 \quad \text{hPa.} \qquad (2)$$

Coefficients (β's) for the barometer effect correction were derived by a correlation analysis between *P* and *W*'s as tabulated in Table III. Then using the coefficient, the barometer corrected relative intensity (W_P) is obtained by

$$W_P = 10^2 \times (W - \beta \times (P - P0)) \quad \text{in units of 0.01\%.} \qquad (3)$$

The value of *P0* is set to 1000.0 hPa for simplicity, though the yearly average of the atmospheric pressure is 1010 hPa.

d. Calculation of daily table

Hourly values of W_P, daily sum and average as well as the 1st, 2nd and 3rd harmonic coefficients of the daily variation of cosmic-ray intensities are computed and tabulated on daily basis. In the same table, the residual dispersion of the cosmic-ray intensities for one day after removing the daily variation (up to 3rd harmonics) is tabulated.

e. Final data file

These hourly values of W_P processed by Online PC are plotted regularly for every solar rotation period using the computer systems in the Laboratory and in Nagoya University Computation Center. Careful check of the data was made, utilizing the hourly data tables and inspecting visually the plotted diagrams. These data are then edited to a final electric data file to be opened in the Data Server of the Laboratory (*cf.* App.II). In the course of the observation renewal and high voltage readjustment of phototubes and repair of amplifiers etc changed counting rates of related components. Such level changes are not adjusted.

Table III. Coefficients for barometer effect correction.

Component	Coefficient β
Vertical	−0.12%/hPa
30°N, E, S and W	−0.12%/hPa
39°NE, SE, SW and NW	−0.12%/hPa
49°N, E, S and W	−0.12%/hPa
64°N, E, S and W	−0.15%/hPa

IV. METHOD FOR ELIMINATING TEMPERATURE EFFECT ON COSMIC-RAY MUON INTENSITY, AND G- AND GG-COMPONENTS

Correction for the atmospheric temperature effect was not applied to the reduced data due to the lack of enough data about the change of the temperature in upper atmosphere. This disadvantage for the muon intensity in comparison with the neutron can be eliminated easily if one takes differences between the data of pairs of components, such as *30°N–30°E*. This difference method is particularly useful for the analysis of cosmic-ray anisotropy, in which the lack of the knowledge about the daily variation of the atmospheric conditions usually casts some doubt on the obtained results. Further, this method eliminates the contamination due to the day to day intensity variation in the analysis of cosmic-ray anisotropy.

Especially, if one takes the second order difference

$$G = (30°N - 30°S) + (30°N - 30°E)$$
$$GG = (49°N - 49°S) + (49°N - 49°E), \qquad (4)$$

the spurious variations from these sources are almost eliminated *(Nagashima et al., 1972)*. Actually the intensity variation of these *G*- and *GG*-components mainly reflects change of difference between the intensity from north polar direction and that from a direction parallel to the equatorial plane. So it is a good index to study the North-South (or North-Equatorial) asymmetry of the cosmic-ray flux. As an example of this characteristic, the annual change of the diurnal variation of *G*-component is shown in Fig. 11. A significant annual change of the amplitude and phase of the diurnal variation indicates the presence of $P_2^1(\sin\lambda)$ type anisotropy in the equatorial coordinate system (λ, φ), due to a $P_2^1(\cos\lambda)$ type anisotropy in interplanetary space. It was concluded that this anisotropy was produced by a pitch angle (χ) distribution of cosmic-ray particles about the interplanetary magnetic field lines from a detailed study of the phenomena *(Nagashima et al., 1972; Fujii, 1971)*.

In Fig. 12, the distribution of the daily values of *G*-component relative to the average over a solar rotation period is plotted for (a) the days when the polarity of the interplanetary magnetic field was towards the sun, and (b) the days when the polarity was away from the sun. A marked difference between two distributions is an indication that the cosmic- ray anisotropy perpendicular to the ecliptic plane has a correlation with the polarity of the interplanetary magnetic field *(Kondo et al., 1975)*. Fig. 13 shows the time variation of daily mean values of *GG*-component in a period of solar rotation number 1939, which demonstrates good correlation between the change of sign of *GG*-component and that of the polarity of the interplanetary magnetic field. Several reasons for this phenomenon, such as the radial density gradient of the cosmic-ray particles *(cf. Swinson, 1969)*, and the tilt of the magnetic field line relative to the ecliptic plane are under critical examination.

For this convenient nature of the *G*- and *GG*-components, they are plotted in the diagrams together with other components.

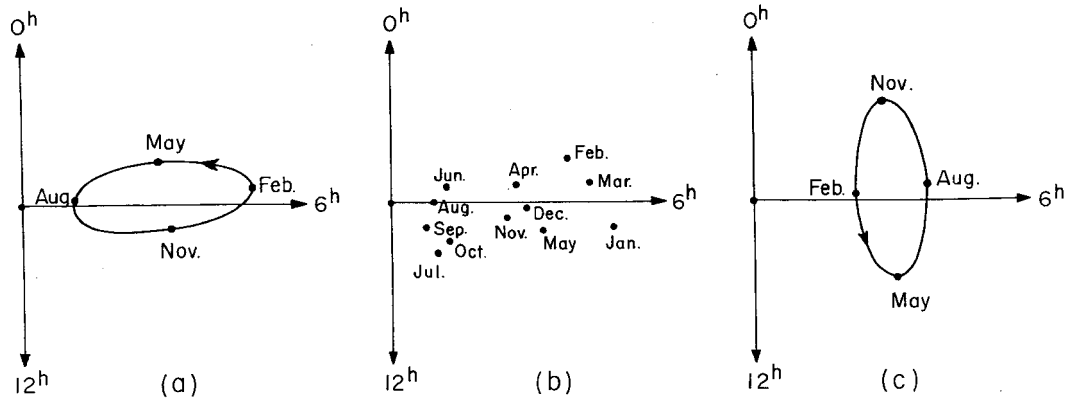

Fig. 11. Annual change of the diurnal vector of *G*-component observed in 1970-1972 is shown in (b). (a) is the prediction on the annual change of the diurnal vector of *G*-component based on the pitch angle distribu-tion hypothesis, while (c) is that based on the density gradient hypothesis

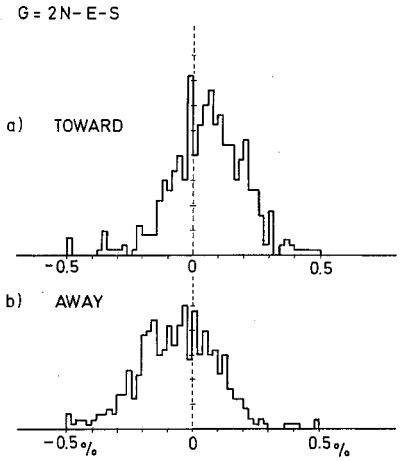

Fig. 12. Distribution of the daily values of G-component relative to the average over a solar rotation period, classified by the polarity of the interplanetary magnetic field

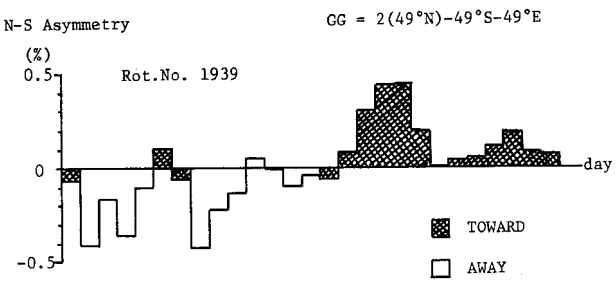

Fig. 13. Transition of N-S asymmetry of *GG*-component correlated with the polarity of the interplanetary magnetic field during one solar rota-tion

V. DESCRIPTION OF DIAGRAMS

a. MULTI-DIRECTIONAL HOURLY MUON INTENSITY

Hourly values of W_P for 14 components are plotted in Diagrams, one for each of Solar Rotation Number. On each diagram, data of 13 components are plotted in the same frame by the following order: *64°E, N, S* and *W; 49°E, N, S* and *W; 30°E* and N; *Vertical*; *30°S* and W; and those of *G*-component *(cf.* IV) are in a separate frame. Data of *39° NE, SE, NW* and *SW* are omitted because of limited space. This ordering was chosen so that the effective rigidity for each component (considering the coupling coefficient) is higher for the components plotted at higher position.

The name of the observation site, the reference level *P0* for the pressure correction and the geographic coordinates are written at left top corner of the diagram. Solar Rotation No. for the particular diagram is written at the center of the diagram, while the first and last dates of the period are written at right top corner. At the top of the frame, the day of the rotation, starting from 1 and ending at 27 for every solar rotation period, is written, while the day of the month is written at the bottom of the diagram together with the name of the month. Time scale of the diagram is in *U.T.*, and 0 hr of the local time corresponds to 15 hr *U.T.* of the previous day.

All data are plotted in the same scaling units as illustrated at left bottom corner of the diagram. In other words, the distance between two adjacent level lines corresponds to 2.8% of intensity change. The level line for each compo-nent expresses the average intensity of all the hourly values over the solar rotation period, the value of which is written in units of percent *(i.e.* $W_P \times 100$) under the name of component at the left side of the frame. At right side of the diagram, the standard error ($\pm\sqrt{N0}$) for hourly value of each component is illustrated.

b. SOLAR ROTATION DIAGRAM OF COSMIC RAYS

This diagram was prepared to emphasize the 27-day recurrence tendency in cosmic-ray intensity and its anisotropy. The hourly values of W_P of *Vertical* component for the specified 14-solar-rotation period, covering about one solar calendar year, are plotted against the day of the rotation on each of Diagrams. At right top corner, the first and last dates of the data in the diagram are written, while those for each rotation period are written at the right side of the frame. Level line for each rotation expresses the average intensity of all hourly values over the particular rotation period, the value of which is written in units of percent *(i.e.* $W_P \times 100$) under the solar rotation no. at the left side of the level line. Again

the scaling unit for the plotting is shown at the left bottom corner of the diagram, and the distance between two adjacent level lines corresponds to intensity change.

Hourly values of W_P of *G*-component in the same period are plotted in Diagrams with the same format as for the *Vertical* component. In the diagrams, the variations for *G*-component are very small in comparison with those for *Vertica*l-component. This is due to the insensitivity of *G*-component to the change of atmospheric condition as well as the day to day modulation of primary cosmic rays as stated in IV.

Differences of hourly values *V–64°E* (=*Vertical –64*°E) are plotted in Diagram with the same format. *V–64°E* is a good index to study the North-South asymmetry in conjunction with *G* and *G*G, as *V–64°E* reflects mainly change of the North-South asymmetry while *G* and *GG* reflect change of the North-South as well as the North-Equatorial asym-metry.

Daily mean of *GG*-component are plotted in Diagram as an index of the polarity of the Interplanetary Magnetic Field *(cf.* IV).

c. MULTI-DIRECTIONAL DAILY MEAN MUON INTENSITY

Daily averages of Wp for 14 components are plotted in Diagrams. One each diagram, data of 13 components are plotted in a frame with the same order as in the hourly value plot *(cf.* VI-a), and those for *G*-component are in a separate frame. The first and last dates of the period covered by a diagram are written at right top corner of the diagram. At the top of the frame, solar rotation numbers are written for each 27-day period. All data except G-component are plotted in the same scaling unit as illustrated at left bottom corner of the upper frame, and the distance between two adjacent level lines corresponds to intensity change. The ordinate scale for *G*-component is expanded twice, as the day to day variation of *G*-component is quite small. The level line for each component expresses the average of daily means over the whole period in the dia-gram, the value of which is written under the name of com-ponent at left side of the diagram.

The annual variations of cosmic-ray intensity for the 13 components in the upper frame are mainly due to the effect of the atmospheric temperature, while those for *G*-component is due to the variation of the North-South (or North-Equatorial) asymmetry of primary cosmic rays *(cf.* IV).

d. SUMMATION HARMONIC DIAGRAM OF COSMIC-RAY DAILY VARIATION

First, second and third harmonic vectors of the daily variation of 5 components *(Vertical, 30°N, E, S* and *W*), averaged over each rotation period are plotted respectively in Diagrams. Each diagram consists of three summation diagrams, grouped on the 14-solar-rotation basis. Vectors (C_{Mi}, S_{Mi}) for *i*-th rotation period are summed up in the diagram, so that *j*-th point in the diagram has the following coordinates.

$$SC_{Mj} = \sum_{i=1}^{j} C_{Mi} \quad ,$$
$$SS_{Mj} = \sum_{i=1}^{j} S_{Mi} \quad for\ j = 1,2,\cdots,14 \qquad (6)$$

The scaling units of axes of summation diagrams are shown in the title of each diagram. The following symbols are used to specify the name of components: □; *Vertica*l, ○; *30°N*, ×:*30°E*, +; *30°S*, and △; *30°W*, respectively.

Acknowledgements:

These data are published on one of projects to con-struct data bases in Center for Joint Observations and Data Processing, Solar-Terrestrial Environment Laboratory, Nagoya University. The graphs are processed using the facilities of Solar-Terrestrial Environment Laboratory and Nagoya University Computation Center.

References

Finch, H.P. and B.R. Leaton (1957): Mon. Not. Roy. Ast. Soc. Geophys. Suppl., **1**, 314.

Fujii, Z. (1971): Rep. Ionos. Space Res. Japan, **25**, 242.

Kondo, I., Z. Fujii and K. Nagashima (1975): Proc. 14th Int. Cosmic Ray Conf., Munich, **4**, 1182.

Nagashima, K., K. Fujimoto, Z. Fujii, H. Ueno and I. Kondo (1972): Rep. Ionos. Space Res. Japan, **26**, 31.

Swinson, D.B. (1969): J. Geophys. Res., **74**, 5591.

Wada, M. (1957): J. Sci. Res. Inst., **51**, 201..xvii

App. I REPLACEMENT OF COINCIDENCE SYSTEM

In September 1979 telescope coincidence system was replaced by a new system, to renew electronic circuits which had been used since the start of observations. Observations restarted on September 30, 1979.

The new coincidence system was designed, modifying the original system to reduce number of sets of coincidence and to simplify electronic circuits. For components from *Vertical* to *39° North-West* in Table II, the logic of new sys-tem is identical with that of the original system. For Components with zenith angles of 49° and 64°, sets of coin-cidence were designed based on 6 m ^{2} detectors units in line on each layer. In Fig. 15 examples of relative positions between upper and lower trays for the coincidence are shown for two representative components, *49° South* and *64° Sout*h. It is noted here that, by the change of coinci-dence system, the total solid angles of components with 49°and 64° zenith angles are increased in comparison with those of the previous system. Average counting rates for the components are shown in Table V. The geometrical para-meters will be reported in the future publication.

Fig. 14. Examples of relative positions between upper and lower detectors for the

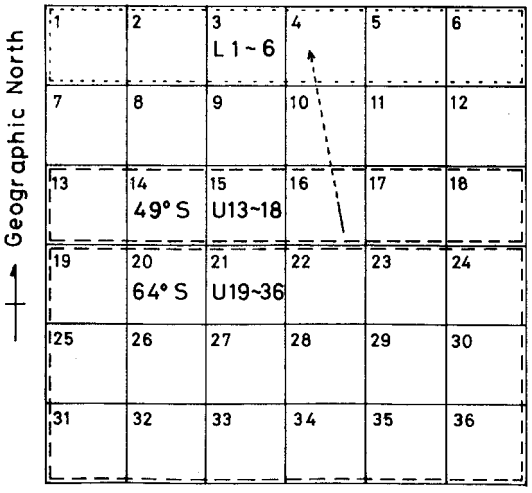

coincidence are shown by broken and dashed rectangu-lars with symbol *L1 ~ 6* and *U13 ~ 18* for *49° Sout*h, and with symbol *L1 ~ 6* and *U19 ~36* for *64° Sout*h. All combinations of coincidence for the components are as follows;

Component	Combination of coincidences
49°S	(L1~ 6) ×(U13 ~ 18) + (L7 ~ 12) ×(U19~24) + (L13 ~ 18) ×(U25 ~ 30) + (L19 ~ 24) ×(U31 ~ 36)
64°S	(L1 ~ 6) ×(U19 ~ 36) + (L7 ~ 12) ×(U25 ~ 36) + (L13 ~ 18) ×(U31 ~ 36)

Table V. Observed average counting rates after replacement of coincidence system

Components	Average count no. (x10^6/hour)
49° North	0.611
49° East	0.581
49° South	0.599
49° West	0.617
64° North	0.178
64° East	0.173
64° South	0.176
64° West	0.180

App.II FOR USE OF DATA

Data of Nagoya Multi-Directional Muon Telescope published so far are available from Home Page of Solar-Terrestrial Environment Laboratory *(http://www.stelab.nagoya-u.ac.jp*) via network with forms of the graphs as well as files of hourly value data, W_P. One record of the hourly value files (96 byte) consist of 24 data of 4 digits each shown below.

Digit	Data
1 - 4	Year
5 - 8	Day of Year
9 - 12	Hour and minute (start time of record)
13-16	Upper Single
17-20	Lower Single
21-24	Vertical
25-28	30° North
29-32	30° East
33-36	30° South
37-40	30° West
41-44	39° NE
45-48	39° SE
49-52	39° SW
53-56	39° NW
57-60	49° North
61-64	49° East
65-68	49° South
69-72	49° West
73-76	64° North
77-80	64° East
81-84	64° South
85-88	64° West
89-92	Pressure
93-96	G-component

You are welcome to use Nagoya Muon Telescope data under the conditions: 1) to acknowledge Cosmic Ray Section, Solar-Terrestrial Environment Laboratory, Nagoya University in any publised use of the data, 2) to send a copy of any paper using these data to:

Z. Fujii
Solar-Terrestrial Environment Laboratory,
Nagoya University, Nagoya 464-8601 Japan
fujii@stelab.nagoya-u.ac.jp